Contractile Vacuole and Papilla drive Cyst/Telotroch transition in *Vorticella microstoma*

Author names.

Eric Galiana, Marie-Line Kuhn, Agnès Attard

Affiliations.

Université Côte d'Azur, INRAE, CNRS, ISA, Sophia Antipolis, France.

Corresponding author.

Eric Galiana, eric.galiana@inrae .fr

Present/permanent address

Institut Sophia Agrobiotech, 400 route des chappes, BP 167, 06903 Sophia Antipolis Cedex FRANCE

ASTRACT

The cyst of the protist ciliate Vorticella efficiently differentiates into teletroch, the free-swimming stage. Here, using video microscopy and quantitative imaging we establish that the cyst differentiation follows two strict temporal and spatial patterns. The temporal pattern is initially marked by the functional formation of the contractile vacuole, which then discharges its fluid into the neoformed cytopharynx and, in a third stage, into a membrane invagination which, to the rhythm of the vacuole, differentiates into an oral cavity exhibiting a polarized cilia array revealed by α-tubulin immunostaining. Two poles delineate the spatial pattern. The apical pole is defined by the position of the pre-existing papilla, which determines the site of oral cavity formation directly below it. The second basal pole is placed at the rupture point of the cyst wall. It is characterized by β-actin accumulation and allowed release of the telotroph according to its basal-apical polarity. Both the temporal and spatial patterns are impaired by concanamycin A treatment, a specific inhibitor of vacuolar type H^+-ATPases altering functions of contractile vacuoles. The findings indicate that cyst to telotroch transition is predetermined by the location of the papilla on the cyst wall and under the control of a functional contractile vacuole. We propose that *Vorticella* cyst is a simple single-cell model for investigating basic principles of integrative neogenesis of organelles in Protozoa, and of apical-basal cell polarity in Eukaryotes.

INTRODUCTION

Van Leeuwenhoek (1677) observed with his light-refracting lens microscope the first microbes, presumably a *Vorticella*. He described them as poor little creatures living in rainwater, having a round or oval body, moving or harpooning themselves towards the extremity, where they possess a contractile tail (stalk), and clumping together in a few filaments. The *Vorticella* genus is now a gathering of more than 100 different sessile peritrich ciliates (Sun et al, 2013). They evolve in marine, freshwater and terrestrial environments, moving or being attached to various substrates such as plant/animal surfaces and appendages, biofilms, flooded objects (Liao *et al.*, 2018; Galiana *et al.*, 2011; Davis and Gloege, 2024). They have been characterized as dominant protozoan species putatively playing a role in fertilization on N supply in rhizosphere soil during the initial growth of *Beta vulgaris L.* (Zeng *et al.*, 2020), and as potential biocontrol agents against plant-parasitic nematodes (Rostami *et al.*, 2022).

At the cellular level, they develop at least in three single-cell forms: free-swimming telotrochs, sessile stalked trophonts and cysts, the last ones being formed under adverse environmental conditions such as lack of nutrients or oxygen, drought, osmotic stress and extreme temperatures (Finley and Lewis, 1960; Bramucci and Nagarajan, 2004; Ryu *et al.*, 2017). The free-swimming telotroch (0.2-1 mm/s in speed) has generally an inverted bell-shaped morphology with an apical part surrounded by at least two rings of cilia emerging from the peristome, which surrounds the open oral cavity/mouth. Immediately behind, the cytopharynx, resulting from a plasma membrane invagination, connects together the oral cavity, particularly, to the food vacuoles, the digestive organelles, as well as the single contractile vacuole (CV). The osmoregulatory CV presumably emptying its contents into the cell's cytopharyngeal region through an elongated tube (Allen and Naitoh, 2002). The cell show the presence of a micronucleus and a polylobar macronucleus and the other eukaryotic organelles. The trophont sessile form has the same morphology and exhibits a retractile stalk (100-150 µm) with which the cell is attached to a surface. The water vortex flow generated by oral cilia beating results in drawing bacteria food particles toward the peristome and then to food vacuoles ingesting particles using phagocytosis. *Vorticella* species with their trophont-stalk contracting almost instantly (10-20 mm/s) and the high swimming speed (0.2-1 mm/s) of

69 the free telotroph are among the fastest cellular micromachines making them highly attractive
70 models for studying movements from hydrodynamic, cellular and molecular point of views
71 (Kamiguri et al, 2012; Ryu *et al.*, 2017; Lisicki et al, 2019; Lupatelli *et al.*, 2023).

72 Perhaps because cyst formation is a slower process, the dynamics of encystment occurring
73 upon adverse conditions, and excystment, allowing telotroch release from the cyst, are less
74 documented. (Warren, 1986). Cyst formation results to the formation of an envelope, the cyst
75 wall, encapsulating a diffuse cytoplasm/hyaloplasm with indistinct cilia, peristome,
76 cytopharynx and vacuoles. Upon favourable conditions, excystment is induced and
77 characterized by cyst differentiation, functional cilia and CV, with osmolarity as a main
78 regulatory factor (Finley and Lewis, 1960).

79 In protists, osmoregulation is achieved by CV which maintains osmotic and ion homeostasis
80 (Plattner, 2013, 2015; Jimenez *et al.*, 2022; More *et al.*, 2024). The cycle of CVs involves three
81 sequential events: diastole (slow extension of the vacuole gradually filled with excess water
82 drained into the endoplasm); systole (rapid vacuolar contraction); and expulsion (the release
83 of vacuolar fluid from the CV outside the cell). To maintain osmotic and ion homeostasis
84 through extrusion of water and excess of ions, the CV may exploit the H^+-gradient generated
85 by the organelle-resident Vacuolar ATPases (V-type H^+-ATPase) (Patterson, 1980; Plattner,
86 2013, 2015). The V-ATPase is highly conserved in eukaryotic organisms and is assembled into
87 two structural multimeric protein complexes: a transmembrane V0-proton pump and a
88 cytoplasmic V1-ATPase that can be reversibly detached and reattached (Wassmer *et al.*, 2006;
89 Wang *et al.*, 2020). In protists as *Dictyostelium* and *Phytophthora* (Temesvari et al, 1996;
90 Mitchell and Hardham, 1999) the function of vacuolar contraction is impaired by
91 concanamycin A, a specific inhibitor of V-ATPases, binding to the V0 subunit c (Huss et al,
92 2002).

93 To date and for a long time ago, knowledge of the *Vorticella* cyst still remains meagre (Warren,
94 1986). The underlying machinery controlling encystment and excystment remains unexplored
95 since the first study of Finley and Lewis (1960). Here, we combine quantitative imaging with
96 drug-inhibited V-ATPase activity to characterize the dynamics of excystment and telotroch
97 release from the *Vorticella microstoma* cyst induced in response to hypo-osmotic conditions.
98 We established that before release, oral cavity and cilia neogenesis, as well as cyst wall
99 deformation follow the redifferenciation of the CV and that their formation is tightly

synchronised both spatially and temporally with the acceleration of the pulsatile rhythm of the diastole-systole-expulsion sequence. We show that inhibition of V-ATPase-mediated proton pumping causes drastic deficits in telotroch release, speed motion as well as cilia organisation and distribution. We propose that *Vorticella* cyst is a simple model for investigating basic principles of integrative neogenesis of organelles in Protozoa, and of basal-apical cell organisation in eukaryotes.

MATERIALS AND METHODS

Vorticella Strain and sample treatment

The *Vorticella microstoma* 30897 stain, in co-culture with *Enterobacter aerogenes (*13048 strain), was purchased from the American Type Culture Collection (ATCC) collection of protists (LGC standards). The cells were cultivated for 3 to 14 days in V8 liquid medium at 24°C. Three days were necessary to observe a high rate of swimming telotroch. Ten to fourteen days were required to reach a 100% rate for cyst formation. In the intermediate range of time, the trophont appeared to be the most common form observed. To induce cyst excystment by means of a hypo-osmotic stress, the medium of 10-14-day-old cultures was discarded and cysts were resuspended in water (the time point t=0 in this study). Samples (100-200 µl) were rapidly mounted in a chamber made of a microscope slides and a top coverslip loaded on two spacers (0,5-1 mm) for starting microscopic observation soon as possible.

To inhibit the V-ATPase, cysts were treated with Concanamycin A, a specific inhibitor of V-ATPases binding to the proteolipid subunit c of the V0 complex (Huss *et al.*, 2002). To assess the function of the CV machinery we proceeded as previously described by Tesmesvari *et al.* (1996) with *Dictyostelium discoideum*. Cysts in the stationary phase were harvested by centrifugation, resuspended in water to create a hypo-osmotic environment and treated or not with 5µM Concanamycin A in solution in DMSO. The appropriate DMSO dilution was applied to the control samples.

Microscopy

Images (size 512×512 or 1029x1044 pixels) and movies (image 512×512 pixels; time scale 0.2 s, time series 1000-3000 s) were obtained using a Zeiss Axio Z1 microscope equipped as followed : a plan-apochromat63x/1.40oil M27 and a EC-plan-neofluofluar 40x.75 M27 objectives; a Hamamatsu camera and the ZEN 2012 pro lite application (Carl Zeiss Microscopy, Germany). The material was available on the Microscopy Platform-Sophia Agrobiotech Institut-INRAE 1355-UNS-CNRS 7254-INRAE PACA, Sophia Antipolis.

136 *Immunohistochemistry*

137 Cysts and telotrochs were collected by centrifugation. They were fixed in methanol for 10 min
138 at -20°C and then incubated in phosphate-buffered saline (PBS), pH 7.2 at room temperature.
139 Samples were treated in PBS with 0,1% Triton for 20 min at room temperature, and later with
140 a blocking solution containing 3% of bovine serum albumin in PBS, for 30 min. They were then
141 first incubated for 18h at 4°C with a rabbit polyclonal antibody against the α-tubulin subunit
142 (NeoBiotech), or against the V1-ATPase B1 subunit (NeoBiotech),or against the β-actin diluted
143 1:200. Samples were washed three times with PBS and incubated for 1 h at room temperature
144 with a FluoProbes 547H Donkey anti-Rabbit IgG diluted 1:200 (Interbiotech – BioScience
145 Innovations). Samples were rinsed three times and mounted in Fluoroshield with DAPI (Sigma,
146 St. Louis, MA USA).

147

148 *Image time series analysis*

149 To analyse CV beating, cytopharynx and oral mouth expansion we proceeded by kymography
150 using in FIJI (Schindelin *et al.*, 2012) the Measurement_Tool plugin (k-button;
151 https://dev.mri.cnrs.fr/projects/imagej-macros/wiki/Velocity_Measurement_Tool). To
152 generate the kymograms, we applied the tool by selecting segmented lines including a
153 diameter and the centre of the vacuole or delimiting as much as possible the mid-section of
154 the papilla, oral cavity, cytopharynx and contractile vacuole. In the kymograms, space was
155 measured along the x-axis while time was measured along the y-axis. To determine mean
156 velocity of cysts and telotrochs, cells were tracked with FIJI using the TrackMate plugin (Ershov
157 *et al.*, 2022) as per the procedure detailed in Lupatelli *et al.* (2023).

158 *Statistics*

159 Experiments were repeated at least 3 times. Data are presented as mean values±SEM. One-
160 way ANOVA with Mann-Whitney pairwise test, were used for the statistical analysis. Past4.17
161 software was used to analyse the data. Bonferroni corrected/adjusted p values of <0.05 are
162 indicated and were considered.

163

164 **RESULTS**

165 *Excystment main features*

166 Encystment and excystment have been reported in several ciliated protists (Li et al, 2022; Jin
167 *et al.*, 2024), in few species within the *Vorticella* genus (Warren, 1986) among which *V.*
168 *microstoma* (Finley and Lewis, 1960) that was investigated in this work. Encystment was
169 induced at a rate of 100% after incubation of *V. microstoma* cells in V8 medium in long-term-
170 culture (10–14 days). At these time-points of incubation, no trophont nor telotroph could be
171 detected with binoculars. The dynamics of encystment was not further examined in this study.
172 To further study the dynamic of excystment, we applied a hypo-osmotic shock to this cyst
173 population. In these conditions, the rate of excystment was estimated at 30% to 50% within
174 1-2 hours. At this time, microscopic observations allowed to establish that the cell released
175 were telotrophs either swimming freely or not. Further investigation on excystment dynamics
176 focused on telotrophs that were not yet swimming and were almost exclusively localized
177 immediately adjacent to the empty cyst wall from which each had emerged. In the results that
178 follow, the timing assigned to each event described refers to the moment (t=0) when osmotic
179 stress was applied.

180 Just before the stress, all *Vorticella* material consisted of perfectly circular and encapsulated
181 cysts (⌀28.8±0.9 µm) with a papilla located at one of its poles as illustrated in Fig. 1A and 1B.
182 At this time (t=0), an immunostaining for the α-tubulin subunit revealed an intracellular and
183 diffuse staining homogeneously distributed in the cytoplasm, suggesting that microtubules
184 were not or poorly polymerised and cilia resorbed (Fig. 1B). Around t=30 min, re-
185 differentiation was initiated as attested by the formation of the contractive vacuole (Fig. 1C)
186 and the cytoplasmic staining for α-tubulin which became punctuated indicating αβ-tubulin
187 oligomerisation in clusters (Fig. 1D). From around t=30-60 min, telotroch release from cysts
188 took place in number. The turgor pressure generated by the telotroph size increase stretched
189 the cyst wall to its maximum capacity up to a breaking point. Cells exhibited the characteristic
190 telotroch bell morphology decorated by cilia (Fig. 1E and 1G). As previously described, their
191 size (1595,5 ± 58,8 μm^2) was significantly increased (p=0,0005; n=14) by 2,4 times compared
192 to cysts (571,2±36,9 μm^2).

193 Immunostainning for α-tubulin (Fig. 1F and 1H) clearly showed occurrence of microtubule
194 polymerisation and cilia neogenesis at the apical side (the oral mouth) of the telelotroph (Fig.
195 1E and 1G), and at its basal side (Fig. 1G). The rupture point of cyst wall at release was detected
196 at the opposite side of the papilla when this one was visible in the plan (Supplementary Fig.
197 1). The position of this point was inscribed in the half-circle opposite to the location of the
198 papilla. This indicated that at the time of rupture, the pressure is exerted differently along a
199 particular cellular axis. Another interesting point is congruent with this hypothesis:
200 systematically, the release of the cell took place according to its apical-basal polarity, its basal
201 end engaging first (Supplementary Fig. 1).

202

203 *Tracking early organelles neogenesis*

204 To examine more precisely, the spatio-temporal dynamics of organelles neogenesis (contactile
205 vacuole, oral mouth, cytopharynx, cilia, cyst wall deformation) within the cyst, samples were
206 positioned in the chamber just after the hypo-osmotic stress. Cysts and excystment were
207 captured at 5 frames per second until telotroch release (Fig. 2; supplementary movies 1, 2 and
208 3). The time series images were processed by kymography. Figure 2 summarises the
209 occurrence of sequential events observed.

210 For the CV, we retrieved from kymograms the number of pulsations before release, kinetics
211 of beating frequency, size of the vacuole at the end of systole (Fig 3). The data show that the
212 time point of the first pulse was variable and detectable quite a long time [7-21 min range]
213 after stress induction (Fig. 3A,B). The total number of pulse before release was constant (41±4,
214 Fig. 3C). Within a range between 0,01 and 0,05 Hz, the contractile frequency distribution
215 overtime reveals for all samples the same pattern: first slow pulsations with a progressive
216 increase in pulse frequencies and then a decrease for the last 5 to 10 ones before release (Fig.
217 3D and Supplementary Fig. 2). These variations are mainly due to variability in diastole
218 duration, while the duration of each systole appears to be very short and constant, estimated
219 in these experiments at 0.8-1 s. As illustrated in Fig 3A, the CV increased in size with time
220 reaching its maximal volume just before release. The overall size was not quantified with
221 kymographic data because vacuole position related to the selected line along the diameter
222 could change marginally due to low flow or Brownian motion acting on the cyst. Changes in

223 vacuole diameter size were manually quantified at three steps: at the first (C_f) and last (C_l)
224 pulse detected within cyst and immediately after release within telotroph (T) (Fig. 3E). At C_l,
225 diameter was approximately 1,9 ($\pm$0,5)-fold larger than at C_f, and 1,6 ($\pm$0,4)-fold larger at T
226 than at C_l. Thus, we can approximate that during differentiation from cyst to telotroch the
227 volume of the CV increased 15 to 20-fold time.

228 Cytopharinx neogenesis was difficult to date precisely. However, when cytopharinx structures
229 were first visualized in several successive time lapse sequences they clearly appeared only in
230 correlation with the ability of vacuole to contraction (Supplementary movie 1, 2 and 3).
231 Moreover, part if not all the vacuole fluid discharge flew into the cytopharinx at systole.
232 Indeed cytopharyngeal volume began to increase on the same frame on which for the first
233 time at the end of diastole, systole started as attested by the decrease of the vacuole volume
234 (Fig. 2A-B and Fig. 4). This increase reached its maximum in the same range of systole duration
235 0.8-1,2 s (Fig. 4A-D) even if here, the frequency of image acquisition did not allow a finer
236 temporal resolution of these two rapid events.

237 Remarkably, our refined temporal analysis also revealed that oral cavity/mouth arise from a
238 thin sheet, that could correspond to a plasma membrane invagination, whose expansion was
239 cadenced by the vacuole contraction (Movie 1, 2 and 3). This primitive thin sheet is first
240 visualized within the hyaloplasm directly and always beneath the papilla (Fig. 2C; Movie 1),
241 probably involving a specialized cell cortex area for anchorage. At this stage, no cilia are visible
242 and appear neither formed nor functional. The sheet gradually individualizes by rhythmic
243 expansion, evolving into a cavity under successive repetitions of vacuole pulsations. The
244 vacuole might empty its fluid into the cytopharyngeal region which joins the oral cavity by
245 forming a tube (Supplementary movie 1). It is also noteworthy to note that when a kymogram
246 was drawn based on a section line crossing organelles from the papilla to the vacuole (Fig. 5A,
247 B), the oral cavity enlargement timely and perfectly coincided with the diastole/systole
248 transition (Fig. 5C). The progressive enlargement could only be detected at the late stages of
249 differentiation. At these stages, the emergence of cilia was detected as shown in Figure 2E-2F,
250 and by the perceptible cilia vibration as the cavity expands just before and after release (Movie
251 1 and 3). Once formed, this cavity constitutes the oral mouth which appears to remain closed
252 throughout the cyst differentiation-telotroch differentiation sequence.

253

254 *Deformation and rupture of cyst wall*

255 At latest stages of cyst differentiation, cyst wall deformation was initiated over a long and
256 variable time [10-200s] before release (Fig. 6A). Sequence images analysis revealed that the
257 cyst wall firstly underwent plastic deformation and then rupture. The plastic deformation
258 exerted all along this time while the rupture was not quantified since it occurred in less than
259 0.2 s, the resolution time of the movies. Plastic deformation resulted from a protrusion at the
260 leading edge taking place in an angular position located in the semi-circle opposite to the
261 papilla coordinates (Fig. 6B) positioning the rupture point for the telotroph release which will
262 follow (Supplementary Fig 1). The plastic deformation resulted with time in an increase in the
263 perimeter of the cyst (Fig. 6C) that could reach just before release 24,2±7,9 µm (Fig. 6D)
264 illustrating the significant elastic/elongation properties of polymers of the cyst wall.
265 Deformation and rupture of cyst wall were associated with local β-actin accumulation
266 revealed by immunostaining just before (Fig. 6 E-G) or during release (Fig. 6 H-J) suggesting
267 that protrusion at the leading edge requires actin filament recruitment.

268

269 *Concanamycin A inhibits cyst differentiation and telotroch release*

270 To initiate exploration of machinery controlling excystment, we assessed the function of the
271 CV complex, the first organelle formed and that seemed involved in cytopharinx and oral
272 mouth neogenesis. The investigation was focused on the V-ATPases generating H^+-gradient
273 across membranes. The V-ATPases are present in abundance in the CV membranes of different
274 protozoa living in a wide range of osmotic environments and important for vacuolar function
275 in expelling water entering the cells by osmosis (Allen and Naitoh; 2002). We first checked if
276 V-ATPases were localized at the CV. We proceeded by immunostaining of cysts and teletroch
277 with a polyclonal antibody against the B1-subunit of the V1-ATPase subcomplex. The results
278 established that in *Vorticella* as in other protists these proteins are plasma and vacuolar
279 membrane-resident (Fig. 7A-D). The typical cressent-like staining of a single vacuole among
280 the food vacuoles and the contractile one strongly indicated that the antibody decorated
281 membranes of the CV. Next, we examined the action of the concanamycin A, a specific
282 inhibitor of the V-ATPases, on cyst differentiation and release. Cysts in stationary phase were
283 collected, washed and then incubated in water in the presence or not of 5 µM concanamycin

284 A. We therefore examined the action of the drug on the function of the CV complex in cyst
285 differentiation and release based on counting in each condition both (i) filled and versus
286 empty cyst walls to calculate the ratio between empty and total cysts numbers (Fig. 7E); and
287 (ii) mean speed of telotrophs in motion (Figure 7F). As expected, no empty cyst wall was
288 detected in cysts at stationary phase (SP; 14-day culture in V8 medium) while a high rate for
289 empty cyst walls was calculated in the control (C) after one hour of release in water. In contrast
290 and at the same time point, in concanamycin A-treated samples (Conca A) the rate of empty
291 cysts was drastically reduced compared to control cells (Fig. 7E). Concomitantly, there was
292 also a marked decrease in the mean speed of moving cells in the presence of the drug (Fig. 7F)
293 indicating that cysts were impaired in the differentiation and/or release processes. Next, we
294 visualized α-tubulin by immunostaining. In the control cells, the α-tubulins were mainly
295 distributed at the two poles of most released telotrochs (Fig. 7G) drawing the characteristics
296 two ciliary arrays of *Vorticella* sp. which promote fluid flow for cell motility; In the
297 concanamycin A-treated cells, cysts and telotrochs were faintly stained compared to the
298 control cells (Supplementary Fig. 3 A,B). The telotrochs could exhibited a staining more
299 uniformly distributed and not reminiscent to a clear polarized status indicating that
300 ciliogenesis, involving polarized basal body docking onto cell membranes, were inhibited or
301 slowed (Fig. 7G). A larger CV could also be observed with an extended systole and no structure
302 reminiscent to the cytopharingal cavity nor ciliated oral mouth (Supplementary Fig. 3, H-L).

303

304 **DISCUSSION**

305 There is today a real Vorticella paradox. Although it was probably the first microorganism
306 described in detail (Van Leeuwenhoek, 1677), *Vorticella sp.* remains a "poor little creature"
307 being among the most neglected organisms in terms of available data in cellular and molecular
308 Biology and Genomics. Only 328 nucleic acid and 9 protein sequences are accessible in
309 databases such as NCBI or Uniprot. It seems not to have yet appeared in the Protist 10 000
310 Genomes Project (Gao *et al.*, 2024). And yet, its distinctive single-celled forms (cyst, telotroph,
311 trophont) make them really suitable objects of investigation on the mechanisms that govern
312 biological transitions within a species. Using microscopy and pharmacology, the current study
313 explored the cyst-telotroph transition in the ciliate Vorticella allowing to excystment.

314 *The cyst excystment of the Vorticella ciliate*

315 (Li *et al.*, 2022) have reviewed a vast amount of information available on changes and some
316 known mechanisms involved during excystment process of 14 representative ciliated protists.
317 General principles on which excystment is induced involved first reappearance of ciliary and
318 intracellular structures that had degenerated during encystment and before excysting.
319 Second, escape from the cyst wall is assisted by a preformed or neoformed pore on the cyst
320 wall and a rupture generated by the pressure of cell movement inside the cyst wall and
321 excystation vacuole. In *Pleurotricha lanceolate,* generation of the pore occurred at uncertain
322 position (Jeffries, 1956).

323 In the current study the data indicate that the papilla and the CV orchestrate a complete
324 differentiation in telotroch from a cyst initially constituted of unstructured
325 hyaloplasm/cytoplasm. They allow us to define two patterns characterizing the cyst transition
326 to telotroph. A first temporal pattern is initially marked by the functional formation of the CV,
327 which then discharges its fluid into the neoformed cytopharynx and, in a third stage, into a
328 membrane invagination which, to the rhythm of the vacuole, differentiates into an oral cavity.
329 The second pattern, a spatial one, is delineated on one pole by the position of the papilla,
330 which determines the site of oral cavity formation and ciliogenesis, directly below it and
331 dictated by the CV tempo. The point of cyst wall rupture, leading to the release of the telotroch
332 in an apical-basal polarity defines the second pole and is characterized by β-actin

333 accumulation. The data emphasizes the role of CV and papilla in the two axes setting up (Fig.
334 8).

335 Indeed, two lines of evidences designate the CV if not the conductor of the establishment of
336 the first temporal pattern, at least as a key upstream player. (i) It is the first functional
337 organelle to emerge. At the strict tempo of its contractions, the appearance of the
338 cytopharynx and then the oral mouth sequentially follow. (ii) Concanamycin A treatment
339 compromising its V-ATPase-dependent functions alters ciliogenesis, polarized ciliary
340 arrangement, release and motion of telotrochs. CV could act by regulating osmotic and ion
341 homeostasis as suggested by the increase in size of released telotroph compared to cyst. It
342 could also act by discharging signaling molecules to the plasma membrane of nascent
343 organelles (cytopharynx , oral mouth), *as D. discoideum* CV discharges cAMP and Ca^{2+} to
344 plasma membrane at the rear of each cell during early cell aggregation allowing stalk
345 formation (Fadil and Janetopoulos, 2021).

346 A passive but key player in the spatial pattern definition is clearly the papilla. Its position
347 initially defines the plasma membrane anchored one where oral mouth will emerge precisely
348 positioned neatly under the papilla. By this way it determines the position of the apical-basal
349 polarity of the neoformed telotroph. Considering that the release always occurred according
350 to the basal-apical polarity of telotroph and within the semi-circle opposite to the papilla,
351 papillae must be considered as the organisers establishing the spatial pattern of excystment.
352 Thus, a papilla position is a reference point of a developmental process and not a simple
353 morphological ornament precious for taxonomy.

354 *Morphogenesis of apical-basal polarity*

355 More broadly, telotroch differentiation in Vorticella should also be a new model to investigate
356 the apical-basal polarity that is essential to many morphogenetic processes in eukaryotes. Its
357 establishment is extensively studied at the genetic and molecular level in higher eukaryotes
358 (Motegi *et al.*, 2020), in ciliates (Soh and Pearson, 2022) or amoebozoa as the unicellular *D.*
359 *discoideum* (Fadil and Janetopoulos, 2021). In *Vorticella* the establishment of apical-basal
360 polarity is achieved within the cyst before release and simply results of a single-cell process
361 primary involving the same two structures, the generative CV and the positional papilla. The
362 pre-existing papilla of the cyst wall is a structural constraint defining the position of the apical

363 organization of future telotrophs through attachment of a particular cortical area of the
364 plasma membrane from which emerges the oral cavity. This could be view as an additional
365 facet of "structural inheritance" whereby in ciliates pre-existing structures enforce a
366 developmental plan for newly formed structures (Beisson & Sonneborn, 1965). In
367 *Tetrahymena pyriformis* and *Paramecium tetraurelia*, the pre-existing intracellular cortical
368 organization of cilia deliver information for the formation and positioning of new structures
369 (basal bodies, microtubular network) defining the cortical organization after scission (Beisson
370 & Sonneborn, 1965; Ng and Frankel, 1977; Soh and Pearson, 2022). It is also reminiscent to
371 maternal tissues acting in higher eukaryotes as a mechanical constraint (Woudenberg *et al.*,
372 2024) as the cell wall-mediated maternal control of apical–basal patterning in brown algae
373 (Shaw and Quatrano, 1996; Dries *et al.*, 2024). The present data clearly indicate that in
374 *Vorticella*, the papilla constitutes the extracellular anchorage point for cellular material
375 assembled during encystment and pre-required for oral cavity and cilia array formation during
376 excystment. Such material could include the fibrillary one viewed after release in Fig. 2F and
377 Movie 1, still linked at the papilla site after release, and conforming to the shape of the thin
378 sheet forming beneath the papilla (Fig2C). The establishment of apical-basal polarity also
379 involves a functional generative CV complex. The analyses of the movies clearly establish that
380 CV expels its fluid through the pore in the cytopharynx. The discharge is then mainly
381 propagated until the papilla-located thin sheet contributing to oral cavity and cilia array
382 formation. The discharge wave did not propagate to the rest of the cell which constitute
383 schematically below the vacuole, the basal side of the cell. Thus cellular process that is
384 happening, it is as though fluid discharge defines a developmental apical way from the CV to
385 the papilla on which cytpharynx and oral mouth genesis take place.

386 *Conclusion*

387 Encystment and excystment are fundamental to the conservation and dissemination of
388 protists in the biosphere. Most of the molecular and cellular associated mechanisms remains
389 elusive. We highlighted generative and structural elements that organise from a cyst and
390 according to a spatio-temporal plan the telotroch differentiation, apical-basal cell polarity and
391 excystment in the ciliate *Vorticella*. By the identification of the papilla as a positional
392 constraint and the CV as a generative organelle of cell polarity in a single-cell system, we
393 provide a new and additional evidence that apical-basal cell polarity is an ancestral trait not

394 only widespread among eukaryotic multicellular cell organisations. Future studies in cell
395 biology will be required to understand how the papilla is formed during encystment, which
396 cellular components are locally recruited to precisely mounted the site of oral cavity and apical
397 cilia array formation, and which CV function(s) (water exclusion, ion homeostasis, signaling
398 molecule driver) controls the cell differentiation.

399

400 **Funding**

401 The work was supported by the National Research Agency; project number ANR22-CE20-
402 0021.

403 **Author contributions**

404 EG and MLK conducted the analyses. EG wrote the first draft. AA and MLK contributed to the
405 writing of the manuscript.

406 **Acknowledgements**

407 A warm thank-you goes to Carlotta Aurora Lupatelli for very fruitful discussions on the topic
408 of the paper.

409

410

411 **REFERENCES**

412 Allen, R. D., and Naitoh, Y. (2002). Osmoregulation and contractile vacuoles of protozoa. Int
413 Rev Cytol 215, 351–94. https://doi.org/10.1016/s0074-7696(02)15015-7

414 Beisson, J., and Sonneborn, T. M. (1965). Cytoplasmic Inheritance of the Organization of the
415 Cell Cortex in *Paramecium Aurelia*. Proc Natl Acad Sci U S A 53, 275–82.
416 https://doi.org/10.1073/pnas.53.2.275

417 Bramucci, M. G., and Nagarajan, V. (2004). Inhibition of Vorticella microstoma Stalk Formation
418 by Wheat Germ Agglutinin. J Eukaryot Microbiol 51, 425–427. https://doi.org/10.1111/j.1550-
419 7408.2004.tb00389.x

420 Davis, A. K., and Gloege, H. (2024). Ciliated Epibionts Modify the Cardiac Stress Reaction to
421 Perceived Predation in Daphnia. Microorganisms 12.
422 https://doi.org/10.3390/microorganisms12061219

423 Dries, E., Meyers, Y., Liesner, D., Gonzaga, F. M., Becker, J. F. M., Zakka, E. E., *et al.* (2024). Cell
424 wall-mediated maternal control of apical–basal patterning of the kelp *Undaria pinnatifida*.
425 New Phytologist 243, 1887–1898. https://doi.org/https://doi.org/10.1111/nph.19953

426 Ershov, D., Phan, M. S., Pylvanainen, J. W., Rigaud, S. U., Le Blanc, L., Charles-Orszag, A., *et al.*
427 (2022). TrackMate 7: integrating state-of-the-art segmentation algorithms into tracking
428 pipelines. Nat Methods 19, 829–832. https://doi.org/10.1038/s41592-022-01507-1

429 Fadil, S. A., and Janetopoulos, C. (2021). The Polarized Redistribution of the Contractile
430 Vacuole to the Rear of the Cell is Critical for Streaming and is Regulated by PI(4,5)P2-Mediated
431 Exocytosis. Frontiers in cell and developmental biology 9, 765316.
432 https://doi.org/10.3389/fcell.2021.765316

433 Finley, H. E., and Lewis, A. C. (1960). Observations on excystment and encystment of *Vorticella*
434 *microstoma*. J Protozool 7, 347–351. https://doi.org/10.1111/j.1550-7408.1960.tb05981.x

435 Galiana, E., Marais, A., Mura, C., Industri, B., Arbiol, G., and Ponchet, M. (2011). Ecosystem
436 screening approach for pathogen-associated microorganisms affecting host disease. Appl
437 Environ Microbiol 77, 6069–75. https://doi.org/10.1128/AEM.05371-11

438 Gao, X., Chen, K., Xiong, J., Zou, D., Yang, F., Ma, Y., *et al.* (2024). The P10K database: a data
439 portal for the protist 10 000 genomes project. Nucleic Acids Res 52, D747–D755.
440 https://doi.org/10.1093/nar/gkad992

441 Huss, M., Ingenhorst, G., König, S., Gassel, M., Dröse, S., Zeeck, A., *et al.* (2002). Concanamycin
442 A, the specific inhibitor of V-ATPases, binds to the V(o) subunit c. The Journal of biological
443 chemistry 277, 40544–8. https://doi.org/10.1074/jbc.M207345200

444 Jimenez, V., Miranda, K., and Augusto, I. (2022). The old and the new about the contractile
445 vacuole of *Trypanosoma cruzi*. J Eukaryot Microbiol 69, e12939.
446 https://doi.org/10.1111/jeu.12939

447 Jin, D., Li, C., Chen, X., Wang, Y., Al-Rasheid, K. A. S., Stover, N. A., *et al.* (2024). Decryption of
448 the survival "black box": gene family expansion promotes the encystment in ciliated protists.
449 BMC Genomics 25, 286. https://doi.org/10.1186/s12864-024-10207-3

450 Kamiguri, J., Tsuchiya, N., Hidema, R., Yatabe, Z., Shoji, M., Hashimoto, C., *et al.* (2012).
451 Contraction behaviors of *Vorticella* sp. stalk investigated using high-speed video camera. II:
452 Viscosity effect of several types of polymer additives. Biophysics (Nagoya-shi, Japan) 8, 11–19.
453 https://doi.org/10.2142/biophysics.8.11

454 Li, Y., Wang, Y., Zhang, S., Maurer-Alcalá, X. X., and Yan, Y. (2022). How Ciliated Protists Survive
455 by Cysts: Some Key Points During Encystment and Excystment. Frontiers in microbiology 13,
456 785502. https://doi.org/10.3389/fmicb.2022.785502

457 Liao, C. C., Shin, J. W., Chen, L. R., Huang, L. L. H., and Lin, W. C. (2018). First molecular
458 identification of *Vorticella* sp. from freshwater shrimps in Tainan, Taiwan. International
459 journal for parasitology. Parasites and wildlife 7, 415–422.
460 https://doi.org/10.1016/j.ijppaw.2018.10.002

461 Lisicki, M., Velho Rodrigues, M. F., Goldstein, R. E., and Lauga, E. (2019). Swimming eukaryotic
462 microorganisms exhibit a universal speed distribution. eLife 8.
463 https://doi.org/10.7554/eLife.44907

464 Lupatelli, C. A., Attard, A., Kuhn, M. L., Cohen, C., Thomen, P., Noblin, X., *et al.* (2023).
465 Automated high-content image-based characterization of microorganism behavioral diversity

466 and distribution. Comput Struct Biotechnol J 21, 5640–5649.
467 https://doi.org/10.1016/j.csbj.2023.10.055

468 Mitchell, H. J., and Hardham, A. R. (1999). Characterisation of the water expulsion vacuole in
469 *Phytophthora nicotianae* zoospores. Protoplasma 206, 118–130.
470 https://doi.org/10.1007/BF01279258

471 More, K. J., Kaur, H., Simpson, A. G. B., Spiegel, F. W., and Dacks, J. B. (2024). Contractile
472 vacuoles: a rapidly expanding (and occasionally diminishing?) understanding. European
473 Journal of Protistology 94, 126078. https://doi.org/10.1016/j.ejop.2024.126078

474 Motegi, F., Plachta, N., and Viasnoff, V. (2020). Novel approaches to link apico-basal polarity
475 to cell fate specification. Current Opinion in Cell Biology 62, 78–85.
476 https://doi.org/10.1016/j.ceb.2019.09.003

477 Ng, S. F., and Frankel, J. (1977). 180 degrees rotation of ciliary rows and its morphogenetic
478 implications in Tetrahymena pyriformis. Proc Natl Acad Sci U S A 74, 1115–9.
479 https://doi.org/10.1073/pnas.74.3.1115

480 Patterson, D. J. (1980). Contractile vacuoles and associated structures: their organisation and
481 function. Biological Reviews 55, 1–46. https://doi.org/10.1111/j.1469-185X.1980.tb00686.x

482 Plattner, H. (2013). Contractile vacuole complex–its expanding protein inventory. Int. Rev. Cell
483 Mol. Biol. 306, 371–416. http://dx.doi.org/10.1016/B978-0-12-407694-5.00009-2

484 Plattner, H. (2015). The contractile vacuole complex of protists--new cues to function and
485 biogenesis. Critical reviews in microbiology 41, 218–27.
486 https://doi.org/10.3109/1040841x.2013.821650

487 Rostami, M., Karegar, A., and Hamzehzarghani, H. (2022). Biocontrol Potential of the Vorticella
488 sp. Isolated from Vermicompost Against Meloidogyne javanica. Current microbiology 79, 333.
489 https://doi.org/10.1007/s00284-022-03030-0

490 Ryu S., Pepper R. E., Nagai M., and France D. C. (2017). Vorticella: a protozoan for bio-inspired
491 engineering. Micromachines 8 ,4. https://doi.org/10.3390/mi8010004

492 Schindelin, J., Arganda-Carreras, I., Frise, E., Kaynig, V., Longair, M., Pietzsch, T., *et al.* (2012).
493 Fiji: an open-source platform for biological-image analysis. Nat Methods 9, 676–82.
494 https://doi.org/10.1038/nmeth.2019

495 Shaw, S. L., and Quatrano, R. S. (1996). The role of targeted secretion in the establishment of
496 cell polarity and the orientation of the division plane in Fucus zygotes. Development
497 (Cambridge, England) 122, 2623–30. https://doi.org/10.1242/dev.122.9.2623

498 Soh, A. W. J., and Pearson, C. G. (2022). Ciliate cortical organization and dynamics for cell
499 motility: Comparing ciliates and vertebrates. J Eukaryot Microbiol 69, e12880.
500 https://doi.org/10.1111/jeu.12880

501 Sun, P., Clamp, J. C., Xu, D., Huang, B., Shin, M. K., and Turner, F. (2013). An ITS-based
502 phylogenetic framework for the genus *Vorticella*: finding the molecular and morphological
503 gaps in a taxonomically difficult group. Proc Biol Sci 280, 20131177.
504 https://doi.org/10.1098/rspb.2013.1177

505 Temesvari, L. A., Rodriguez-Paris, J. M., Bush, J. M., Zhang, L., and Cardelli, J. A. (1996).
506 Involvement of the vacuolar proton-translocating ATPase in multiple steps of the endo-
507 lysosomal system and in the contractile vacuole system of Dictyostelium discoideum. J Cell Sci
508 109 (Pt 6), 1479–95. https://doi.org/10.1242/jcs.109.6.1479

509 Van Leewenhoeck, A. (1677). Observations, communicated to the publisher by Mr. Antony van
510 Leewenhoeck, in a Dutch letter of the 9th of Octob. 1676. Philos. Trans. R. Soc. Lond. 12, 821–
511 831. https://doi-org.insb.bib.cnrs.fr/10.1098/rstl.1677.0003

512 Wang, L., Wu, D., Robinson, C. V., Wu, H., and Fu, T. M. (2020). Structures of a Complete
513 Human V-ATPase Reveal Mechanisms of Its Assembly. Mol Cell 80, 501-511 e3.
514 https://doi.org/10.1016/j.molcel.2020.09.029

515 Warren, A. (1986). A revision of the genus *Vorticella* (Ciliophora: Peritrichida). Bulletin of the
516 British Museum (Natural History) Zoology 50, 1–57. https://archive.org/details/biostor-
517 39/mode/2up

518 Wassmer, T., Kissmehl, R., Cohen, J., and Plattner, H. (2006). Seventeen a-subunit isoforms of
519 paramecium V-ATPase provide high specialization in localization and function. Mol Biol Cell
520 17, 917–30. https://doi.org/10.1091/mbc.e05-06-0511

Woudenberg, S., Hadid, F., Weijers, D., and Borassi, C. (2024). The maternal embrace: the protection of plant embryos. Journal of Experimental Botany 75, 4210–4218. https://doi.org/10.1093/jxb/erae071

Zheng, W. B., Wang, L., Wang, X., Du, M. L., Ge, C., Wang, Q. H., *et al.* (2020). Dominant protozoan species in rhizosphere soil over growth of Beta vulgaris L. in Northeast China. Bioengineered 11, 229–240. https://doi.org/10.1080/21655979.2020.1729929

529 **FIGURES LEGENDS**

530 **Figure 1 - Cysts and telotroch Morphologies**

531 (**A, C, E, G**) Representative images of phase-contrast micrographs 0, 30 and 60 min after
532 induction of the hypo-osmotic stress: cysts (**A, E**), telotrophs (**E, G**). (**B, D, F, H**) Representative
533 images of immunofluorescence of α-tubulin (red) and DAPI staining of polylobar nuclei (blue)
534 in cysts (**B, D**) and telotrochs (**F, H**). Scale bars: 10 µm.

535

536 **Figure 2 - Time-lapse imaging of excystment**

537 (**A-F**) A representative sequence of main events observed during cyst differentiation extracted
538 from the Movie S1. In this movie t=0 was undetermined. Annotation indicates the localisation
539 of the different structures : (p) papilla; (cv) CV; (c) cytophrynx; (m) oral mouth/oral cavity; (n)
540 nucleus; the dotted white line identified the location of cyst wall deformation. The
541 micrographs illustrate different interconnected steps of cyst differentiation: (**A**) the CV during
542 diastole; (**B**) the cytopharynx filling during systole; (**C**) the emergence of a thin sheet beneath
543 the papilla; (**D**) the oral cavity expansion from the thin sheet; (**E**) the cytopharynx and oral
544 cavity connexion, and the cyst wall deformation; (**F**) Basal to apical release. Scale bar: 10 µm.

545

546 **Figure 3 - Kymogram of differentiation from cyst to telotroph.**

547 (**A**) Kymograph generated from Movie S2 showing the kinetics of CV pulses. Inlet shows the
548 position of the section-line selected and the localisation of CV during the first diastole
549 detected. On the kymogram are indicated : (i) the position of CV, (ii) the duration of the first
550 and second diastole detected and (iii) by vertical arrows each pulse serial number positioned
551 arbitrarily at the end of each diastole indicated (**B**) Boxplot of time for detection of a first pulse
552 (n=14). (**C**) Boxplot of number of pulses counted from t=0 to telotroch release (n=14). (**D**)
553 Mean of vacuole contraction frequencies at each pulse time series number (n=9). (**E**) Boxplot
554 of vacuole diameter: within cyst at the first (C_f) and last (C_l) pulse detected and within
555 telotroph (T) immediately after release (Fig. 3E, n=14).

556

557 **Figure 4 - Time-lapse imaging of systole and cytopharynx filling**

558 (**A-D**) Static images in duplicate, without (left) and with annotation (right), and taken in Movie
559 S3 at 0.4-s intervals. Images show the proximal continuity between oral mouth (M),
560 cytopharynx and CV (CV) localisation during the last systole before telotroch release. (**E**) Image
561 shows the last image before a new diastole occurs. Scale bar, 30 µm.

562

563 **Figure 5 - CV punctuates the tempo of enlargement of the mouth being formed**

564 (**A, B**) images indicating how the section line was positioned to generate a kymogram. The
565 section line crosses the papilla (p), oral cavity (m), cytopharynx (c) and CV (cv). (**C**) The image
566 shows the final part of the kymogram including the last eleven contraction of the vacuole
567 before release. Horizontal dotted white bars underline the perfect synchronisation between
568 CV systole, filling of the cytopharynx and progressive and rhythmed oral cavity enlargement.
569 Bold yellow bars illustrate the opening increment of the oral cavity, perfectly rhythmed in a
570 phase pattern with the last vacuolar contractions occurring before release which is indicated
571 by the red dotted line.

572

573 **Figure 6 - Deformation and rupture of cyst wall**

574 (**A**) Time allocated to cyst wall stretching from protrusion emergence to release (n=14). (**B**)
575 Polar plot of angle between papilla position and the rupture point. Range of angles between
576 the half-line passing through the midpoint of the papilla (p; θ=0°) and the center of mass of
577 the cyst, and the half-line passing through the center of mass and the midpoint defined at the
578 site of protrusion emergence initiating the plastic deformation and then release. This range
579 only contains obtuse angle values (n=16). (**C**) Percentage of increase in cyst size resulting from
580 the ratio between the perimeters calculated at the time point just before release and before
581 protrusion occurred (n=8). (**D**) Compute curvature of a perimeter cyst just before release
582 showing local deformation of the cyst wall and the location of the papilla (p) and mouth (m).
583 Calibration bar indicates value for point curvature (μm^{-1}). (**E-J**) Phase contrast (**E-H**), DAPI
584 staining of polylobar nuclei (**F, I**) and β-actin immunostaining (**G, J**) of cysts during release.
585 Scale bars, 10 µm.

586

587 **Figure 7 - Concanamycin inhibits differentiation and release**

588 (**A-D**) Phase contrast (**A, C**) and immunostaining (**B, D**) of a cyst and a teletroch with a
589 polyclonal antibody against the B1-subunit of the V1-ATPase subcomplex. (**E**) Rate of empty
590 cysts and (**F**) telotroch mean speed, at stationary phase (SP), after one hour of release in water
591 in the presence of concanamycin A (Conca A) or not (C for control). (**G**) Phase contrast and α-
592 tubulin immunostaining of representative cysts and teletrochs treated or not with
593 concanamycin A. White stars and "m" annotation indicate the CV and oral mouth position,
594 respectively. Scale bars, 10 µm.

595

596 **Figure 8 - Overview of events that contribute to the formation of telotroch release from a**
597 **cyst in *Vorticella microstoma***

598 A step-by-step schematic diagram of a cyst/telorotroch transition depicting the hypothesis
599 raised in this work according to which within the cyst, the papilla position at the wall cyst and
600 a functional contractile vacuole cause and orient organelles formation (cytopharynx and
601 ciliated oral mouth) as well as apical-basal telotroch polarity, and subsequent telotroch
602 release.

603

604 **Supplementary Figure 1 - Telotroch Release from cyst**

605 Micrographs of six cysts and telotrochs at t=0 (left) and approximately t=50 min (right) just
606 after release. (p) indicates the papilla localisation, and (*) the position where the cyst wall will
607 be (left) and is ruptured (right). The apical-basal polarity of telotrophs is indicated immediately
608 after release illustrating that excystment involves a specific orientation of telotrophs in the
609 opening of the cyst wall with the basal end at first and then the apical end (easily identified by
610 the oral cavity). Scale bar: 20 µm.

611

612 **Supplementary Figure 2 - Kinetics of vacuole beat frequency as a function of the ordered**
613 **series of diastole-systole cycles.**

614 Nine independent time-lapse experiments recording cysts from t=0 to the release time ranging
615 between 20 and 40 min. X-axis indicates the serial number of cycles; y-axis is indicative of the
616 beating frequency between two successive pulses.

617

618 **Supplementary Figure 3**

619 (**A-B**) Merged images of phase contrast and α-tubulin immunostaining of representative cysts
620 and teletrochs treated (**B**) or not (**A**) with concanamycin A. Scale bar: 50 µm. (**C-G**) typical
621 timing of systole duration of 1s with the dynamics of engulfment of the cytopharynx and
622 emergence of oral cavity signed by membrane invagination below the papilla. (**H-L**) Extension
623 of systole duration (7s) with no structures reminiscent to the cytopharingal cavity nor cilated
624 oral mouth in a concanamycin A-treated cyst connection. Scale bar: 10 µm.

625

626 **Movie1 - Time-lapse video microscopy of a cyst differentiating in a telotroch**

627 Images were taken every 500 ms with a 40× objective. t=0 was undetermined. Annotation
628 recordings is frame-by-frame.

629

630 **Movie2 - Video microscopy of a cyst differentiating in a telotroch**

631 Time-lapse imaging with 0.2-s intervals. Images were taken every 200 ms with a 40× objective.
632 The indicated timing is refered to t=0 when the differentiation started in response to hypo-
633 osmotic conditions.

634

635 **Movie3 - Video microscopy of a cyst differentiating in a telotroch**

636 Images were taken every 200 ms with a 40× objective. The indicated timing is refered to t=0
637 when the differentiation started in response to hypo-osmotic conditions.

638

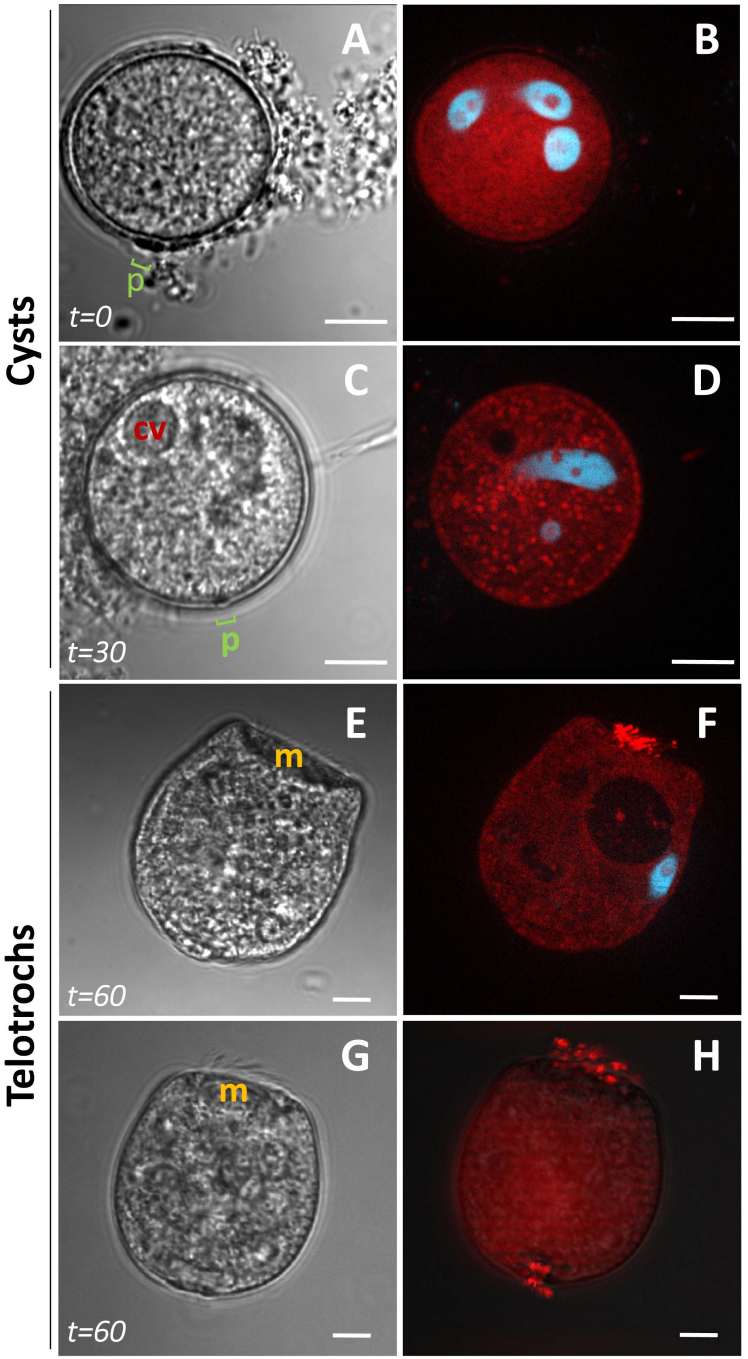

Figure 1

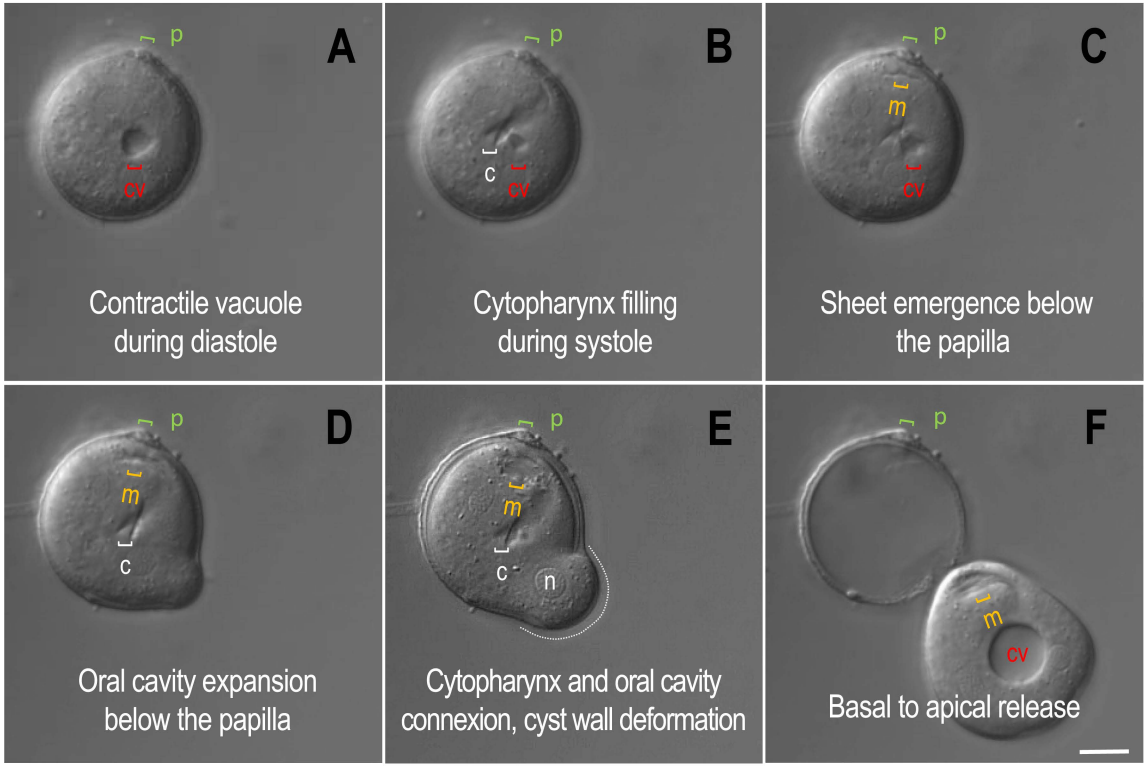
A
p
cv
Contractile vacuole during diastole
B
p
c
cv
Cytopharynx filling during systole
C
p
m
cv
Sheet emergence below the papilla
D
p
m
c
Oral cavity expansion below the papilla
E
p
m
c
n
Cytopharynx and oral cavity connexion, cyst wall deformation
F
p
m
cv
Basal to apical release

Figure 2

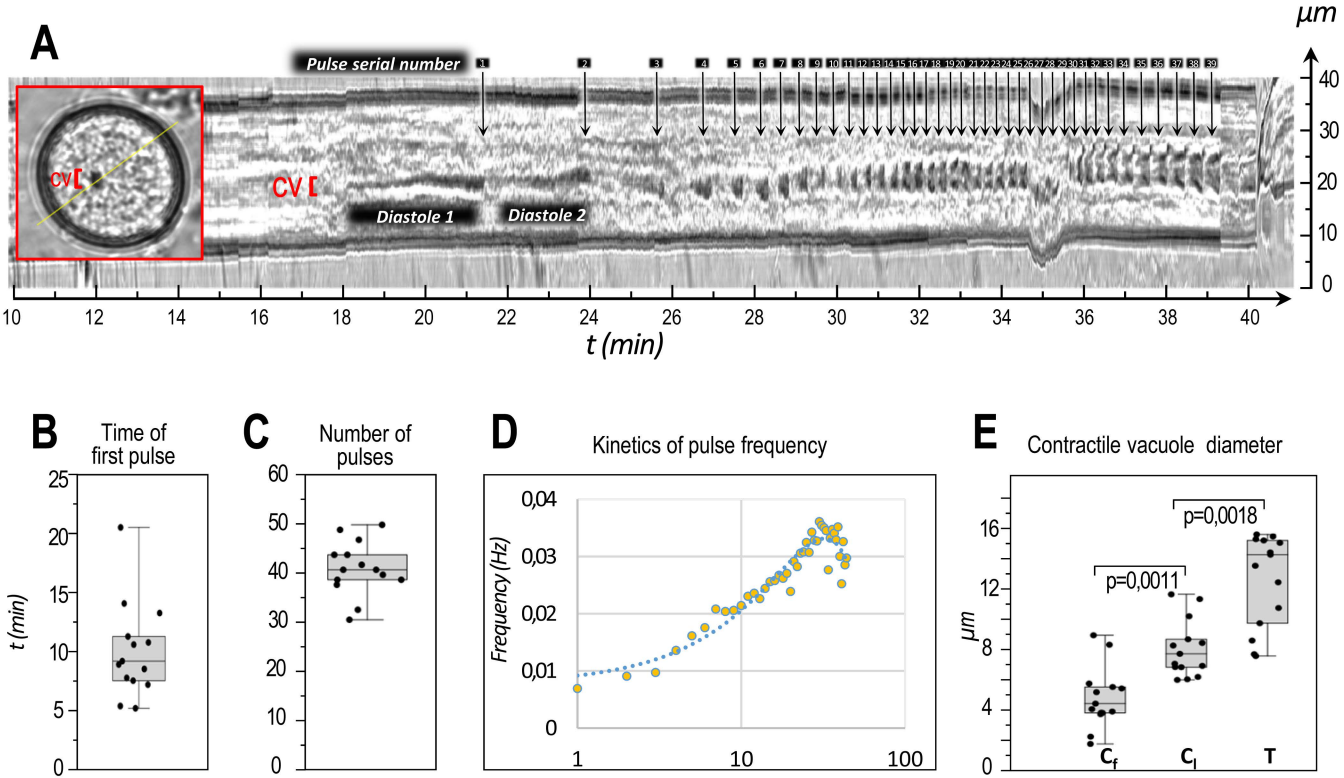
A
Pulse serial number
CV
CV
Diastole 1
Diastole 2
µm
t (min)
B
Time of first pulse
t (min)
C
Number of pulses
D
Kinetics of pulse frequency
Frequency (Hz)
E
Contractile vacuole diameter
µm
p=0,0011
p=0,0018
C_f
C_l
T

Figure 3

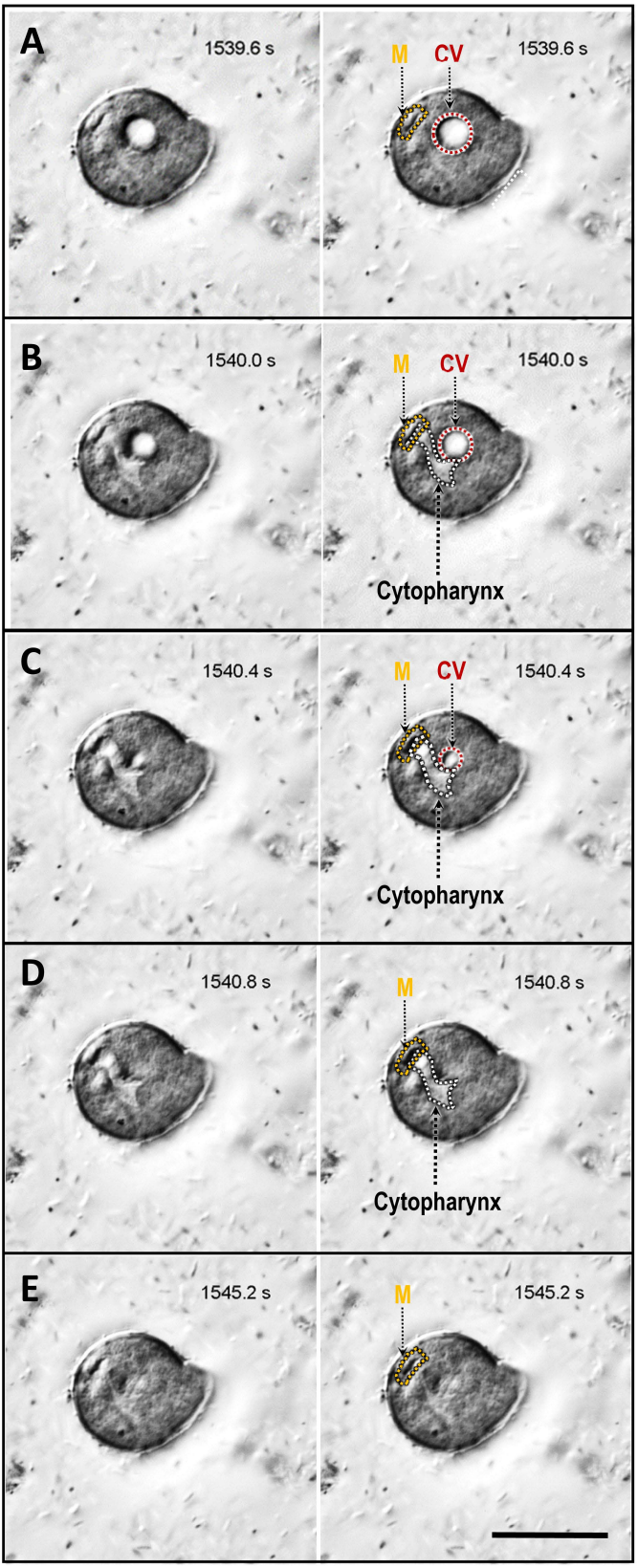
A
1539.6 s
M
CV
1539.6 s
B
1540.0 s
M
CV
1540.0 s
Cytopharynx
C
1540.4 s
M
CV
1540.4 s
Cytopharynx
D
1540.8 s
M
1540.8 s
Cytopharynx
E
1545.2 s
M
1545.2 s

Figure 4

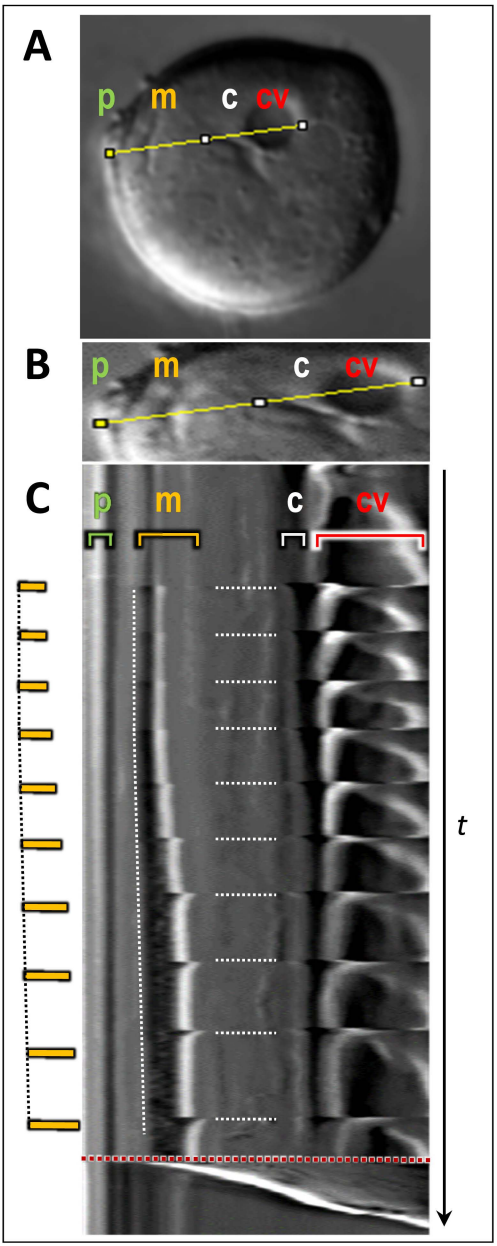

Figure 5

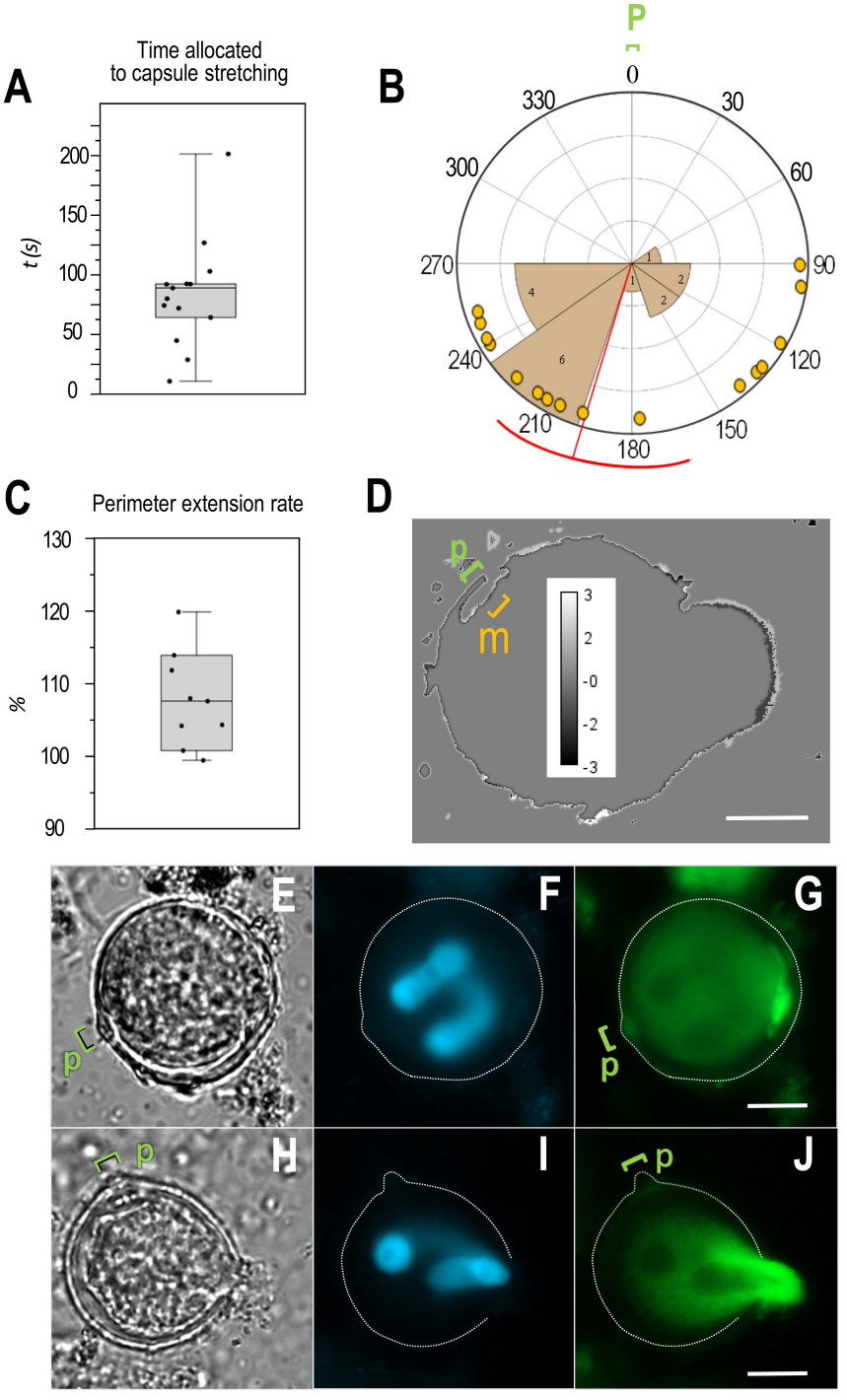
A
Time allocated
to capsule stretching
t (s)
200
150
100
50
0
B
P
0
30
60
90
120
150
180
210
240
270
300
330
1
2
4
6
C
Perimeter extension rate
%
130
120
110
100
90
D
p
m
3
2
-0
-2
-3
E
F
G
H
I
J
p

Figure 6

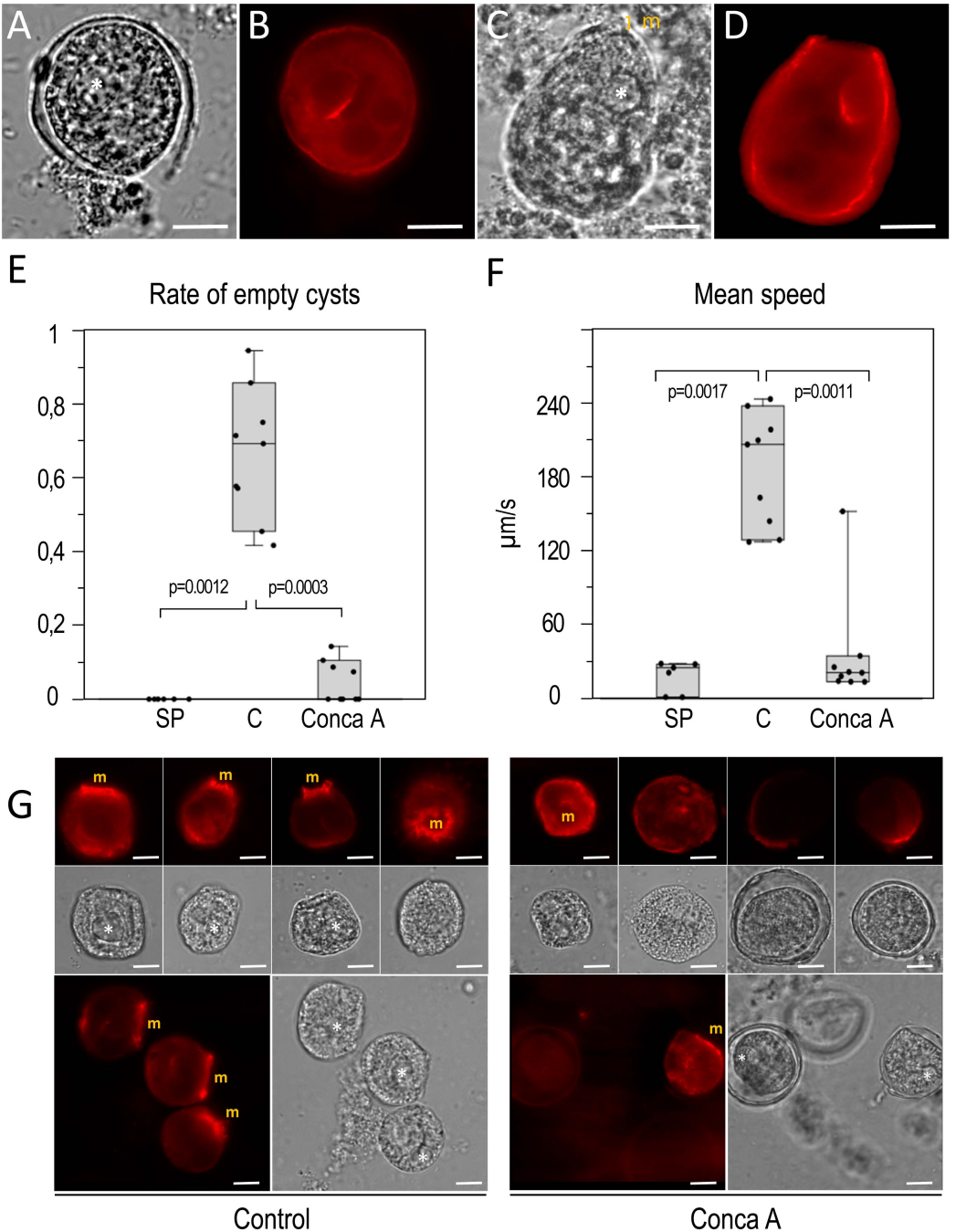
A
B
C
1 m
D
E
Rate of empty cysts
1
0,8
0,6
0,4
0,2
0
p=0.0012
p=0.0003
SP
C
Conca A
F
Mean speed
240
180
120
60
0
µm/s
p=0.0017
p=0.0011
SP
C
Conca A
G
m
Control
Conca A

Figure 7

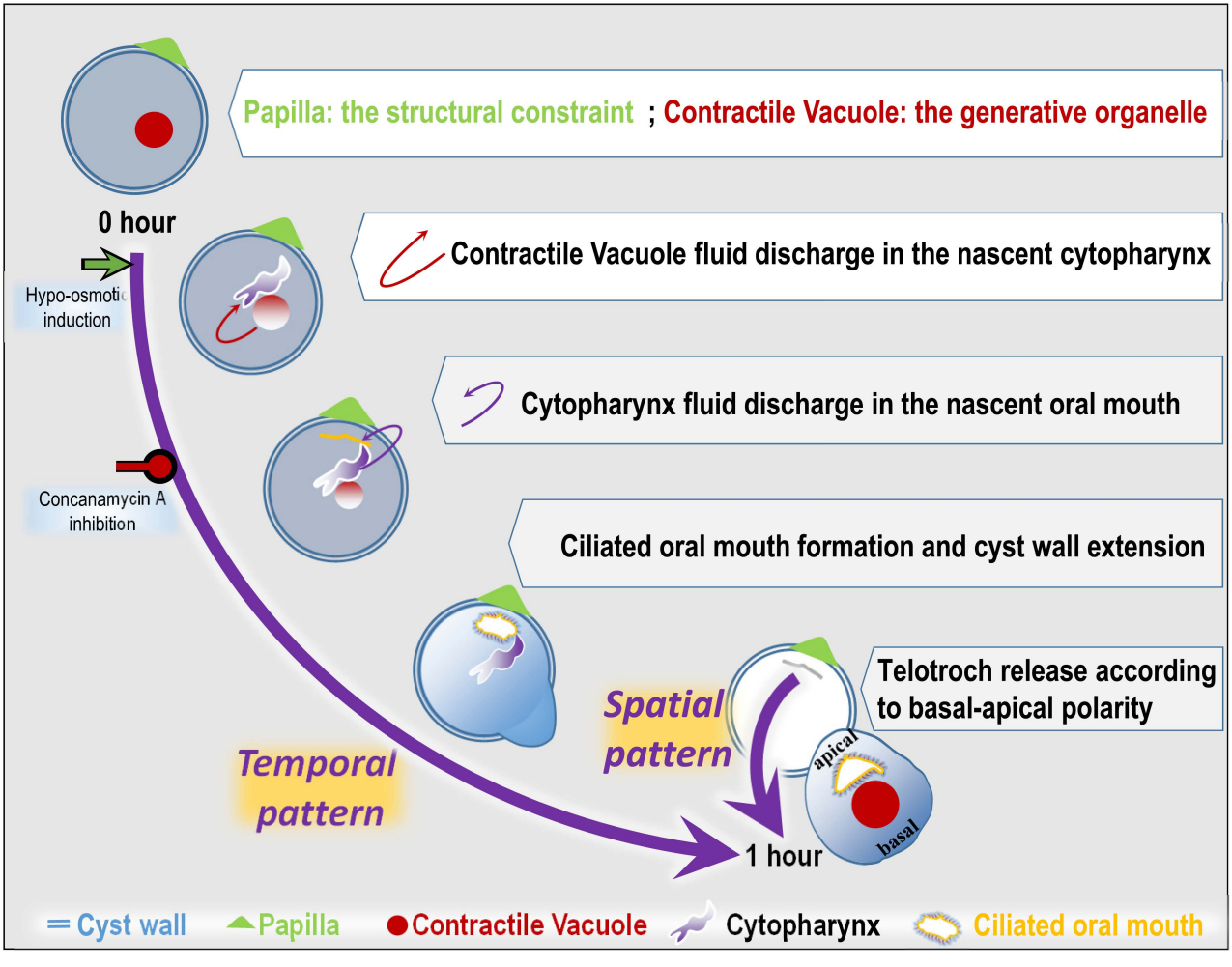
Papilla: the structural constraint ; Contractile Vacuole: the generative organelle
0 hour
Hypo-osmotic induction
Contractile Vacuole fluid discharge in the nascent cytopharynx
Cytopharynx fluid discharge in the nascent oral mouth
Concanamycin A inhibition
Ciliated oral mouth formation and cyst wall extension
Telotroch release according to basal-apical polarity
Spatial pattern
Temporal pattern
apical
basal
1 hour
Cyst wall
Papilla
Contractile Vacuole
Cytopharynx
Ciliated oral mouth

Figure 8

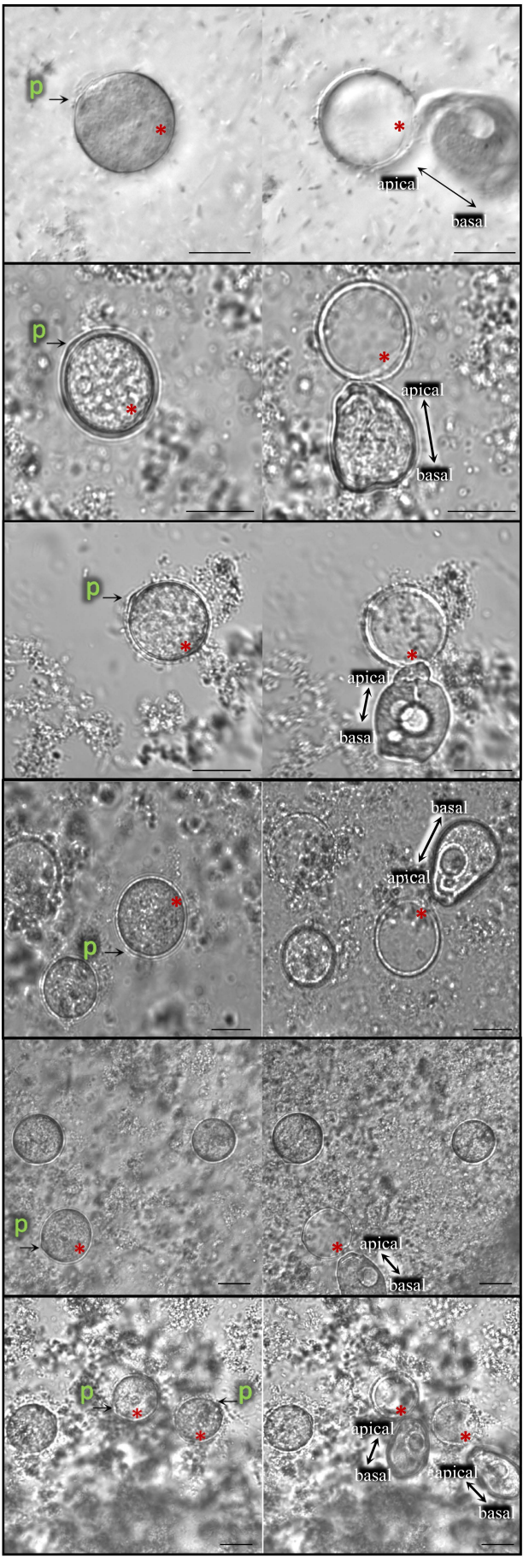

Supplementary Fig 1

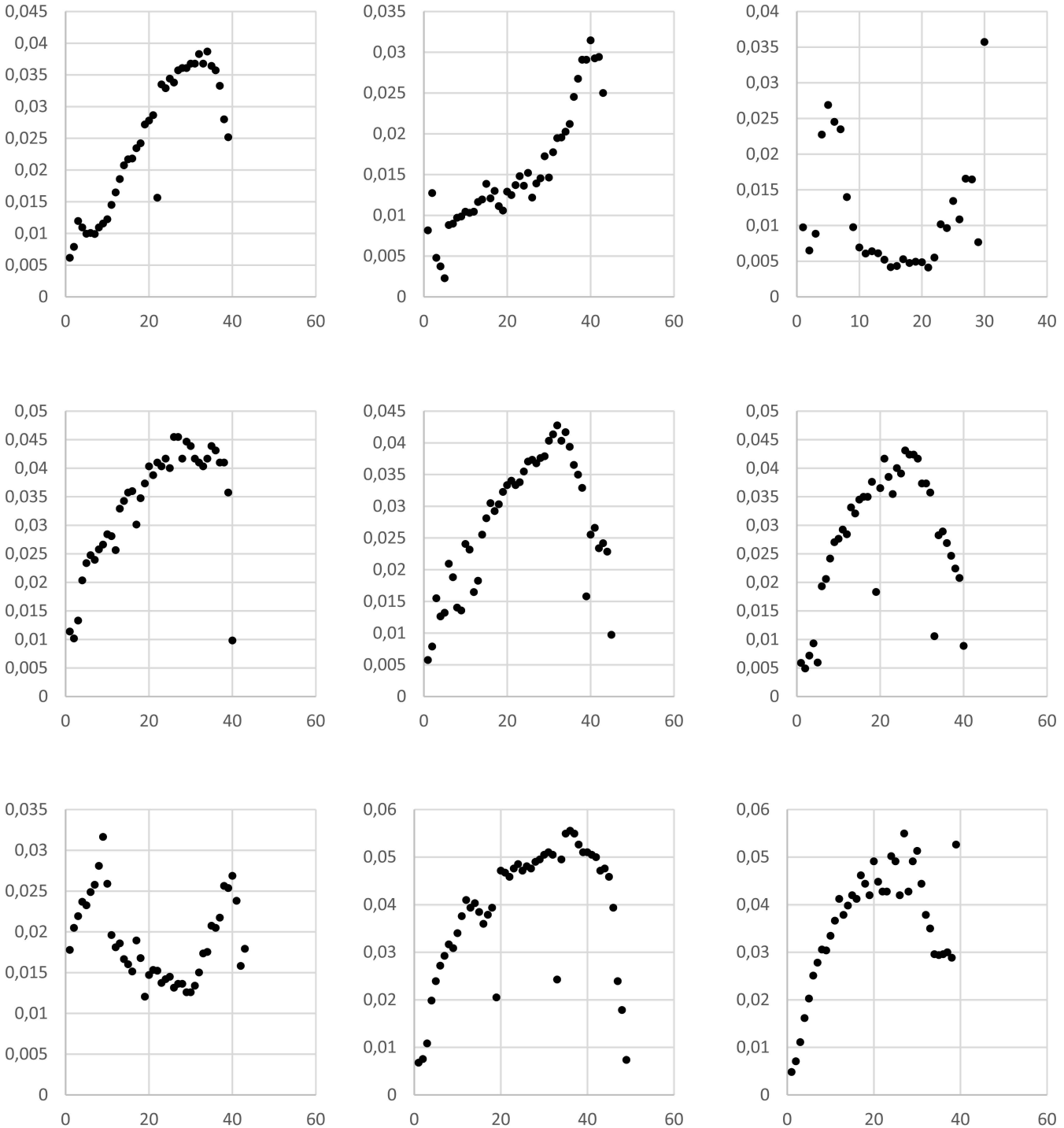

Supplementary Fig 2

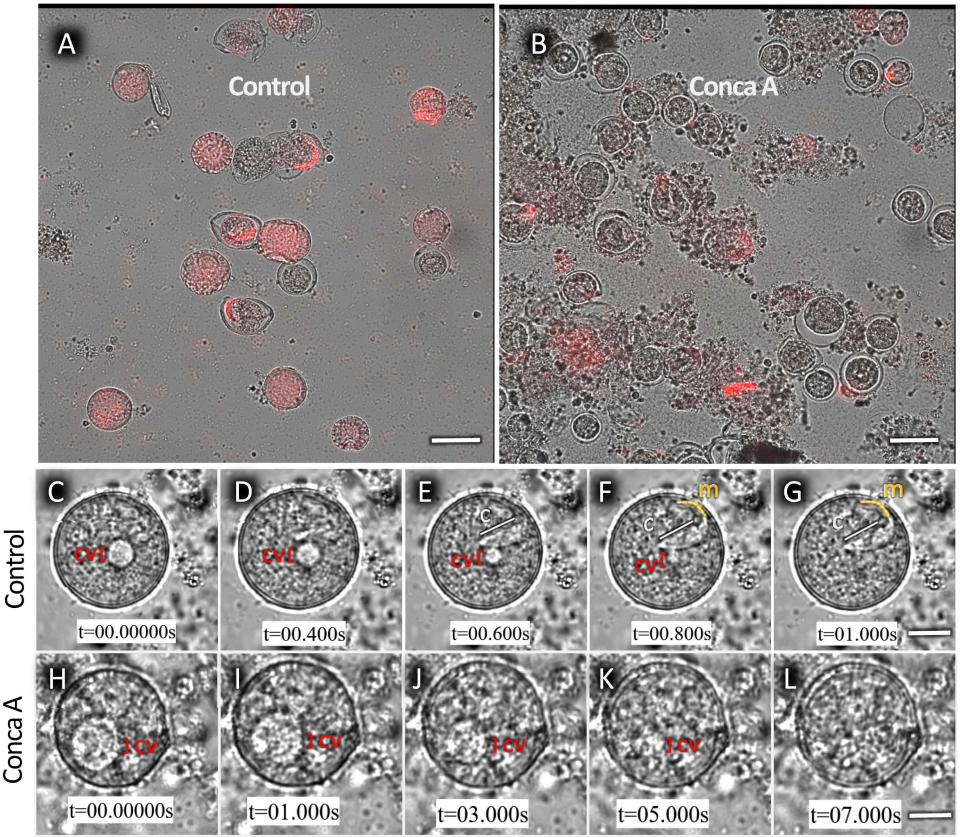

Supplementary Fig 3